Electronic Supplementary Information

Rapid synthesis of high-areal-capacitance ultrathin hexagon Fe_2O_3 nanoplates on carbon cloth via a versatile molten salt method

Yi-Jie Gu[a], Wei Wen[b], Shilie Zheng[c] and Jin-Ming Wu*[a]

[a] State Key Laboratory of Silicon Materials and School of Materials Science and Engineering, Zhejiang University, Hangzhou 310027, P. R. China.

[b] College of Mechanical and Electrical Engineering, Hainan University, Haikou 570228, P. R. China.

[c] College of Information Science and Electronic Engineering, Zhejiang University, Hangzhou 310027, P. R. China.

* Corresponding author

Name: Jin-Ming Wu

E-mail: msewjm@zju.edu.cn

Affiliation: State Key Laboratory of Silicon Materials, Zhejiang University

Contact address: Hangzhou 310027, PR China

Calculation

For MO@CC electrodes, the areal (C_s, mF cm^{-2}) and gravimetric (C_m, F g^{-1}) capacitances are calculated from the corresponding CV curves at different scan rates according to following equations (1) and (2), respectively,

$$C_s = \frac{\int idV}{S \times v \times \Delta V} \quad (1)$$

$$C_m = \frac{\int idV}{m \times v \times \Delta V} \quad (2)$$

where $\int idV$ is the area of CV curve, ΔV is the potential window (V), v is the scan rate (mV s^{-1}), S is the working area (*1 cm^2*), and m is the mass density (Table S1, mg cm^{-2}).

For supercapacitors, the areal capacitance (C, mF cm^{-2}), energy density (E, μWh cm^{-3}) and power density (P, mW cm^{-3}) are calculated from GCD curves at different current densities according to equations (3)−(5),

$$C = \frac{I \times \Delta t}{S \times \Delta V} \quad (3)$$

$$E = \frac{C \times \Delta V^2}{2 \times d} \quad (4)$$

$$P = \frac{E}{\Delta t} \quad (5)$$

where I is the charge/discharge current (mA), S is the working area of electrodes (*ca. 1 cm^2*), ΔV is the potential window (V) during the discharge process (excluding IR drop), d is the thickness of the device (*0.2 cm*), and Δt is the discharge time (s).

For the electro-kinetic study, the power law equation (6) can be used to determine a and b values by taking the current *vs.* voltage response of the electrode active material at various scan rates,[1]

$$i = av^b \quad (6)$$

where i and v are the peak current and the scan rate for the CV measurements, respectively. For a redox reaction limited by a semi-infinite diffusion, b = 0.5; for a capacitive process that corresponds to fast faradic surface controlled energy storage behaviour, b = 1.

The total current i measured at a specific voltage can be separated into two segments which are capacitive (k_1v) and diffusive contribution ($k_2v^{0.5}$), using the following equation (7),[2]

$$i = k_1v + k_2v^{0.5} \quad (7).$$

Table S1. Mass loading of Fe_2O_3 for *x*-Fe_2O_3@CC (*x* = 0.3, 0.6, 0.9 and 1.2 mmol).

Samples	Mass loading of Fe_2O_3 (mg cm^{-2})
0.3-Fe_2O_3@CC	1.18
0.6-Fe_2O_3@CC	1.89
0.9-Fe_2O_3@CC	3.33
1.2-Fe_2O_3@CC	4.70

Table S2. Comparison in the electrochemical performance of the Fe_2O_3-based electrodes in aqueous electrolytes.

Material	Electrolyte	Potential	Scan rate/ Current	Capacity	Ref.
Fe_2O_3 nanoneedles on Ni NTAs	1 M Na_2SO_4	–0.8–0 V	10 mV s^{-1}	418.0 F g^{-1}	3
α-Fe_2O_3/PPy	1 M Na_2SO_4	–0.8–0 V	0.5 mA cm^{-2}	382.4 mF cm^{-2}	4
α-Fe_2O_3@PANI nanowires	1 M Na_2SO_4	–0.8–0 V	0.5 mA cm^{-2}	103.0 mF cm^{-2}	5
Fe_2O_3 nanocrystals	1 M Na_2SO_4	–0.2–1 V	2 mA cm^{-2}	1660 mF cm^{-2}	6
GF/H-Fe_2O_3 nanoplates	3 M KOH	–1–0 V	1 mA cm^{-2}	694.0 mF cm^{-2}	7
Ti-doped Fe_2O_3@PEDOT	5 M LiCl	–0.8–0 V	1 mA cm^{-2}	1150.0 mF cm^{-2}	8
Fe_2O_3/graphene	1 M KOH	–1.05– -0.3V	2 A g^{-1}	908.0 F g^{-1}	9
Fe_2O_3 nanotubes	5 M LiCl	–0.8–0V	1 mA cm^{-2}	180.4 mF cm^{-2}	10
α-Fe_2O_3 nanorods	3 M LiCl	–0.8–0 V	0.5 mA cm^{-2}	382.7 mF cm^{-2}	11
α-Fe_2O_3@NiO	1 M LiOH	–0.2–0.8V	1 mA cm^{-2}	557.0 mF cm^{-2}	12
0.3-Fe_2O_3@CC	**6M KOH**	**–1.0–0 V**	**2 mV s^{-1}**	**1754.9 mF cm^{-2}**	**This work**
0.6-Fe_2O_3@CC				**1762.7 mF cm^{-2}**	
0.9-Fe_2O_3@CC				**4175.7 mF cm^{-2}**	
1.2-Fe_2O_3@CC				**3339.0 mF cm^{-2}**	

Abbreviations in Table S2

NTAs: nanotube arrays, **PPy**: polypyrrole, **PANI**: polyaniline, **GF**: graphene foam, **H**: hydrogenated, **PEDOT**: 3,4-ethylenedioxythiophene.

REFERENCES

1 Z. H. Huang, Y. Song, D. Y. Feng, Z. Sun, X. Q. Sun and X. X. Liu, High mass loading MnO_2 with hierarchical nanostructures for supercapacitors, *ACS Nano*, 2018, **12**, 3557−3567.

2 J. B. Cook, H. S. Kim, T. C. Lin, C. H. Lai, B. Dunn and S. H. Tolbert, Pseudocapacitive charge storage in thick composite MoS_2 nanocrystal-based electrodes, *Adv. Energy Mater.*, 2017, **7**, 1601283−1601295.

3 Y. Li, J. Xu, T. Feng, Q. F. Yao, J. P. Xie and H. Xia, Fe_2O_3 nanoneedles on ultrafine nickel nanotube arrays as efficient anode for high-performance asymmetric supercapacitors, *Adv. Funct. Mater.*, 2017, **27**, 1606728−1606738.

4 L. B. Wang, H. L. Yang, X. X. Liu, R. Zeng, M. Li, Y. H. Huang and X. L. Hu, Constructing hierarchical tectorum-like alpha-Fe_2O_3/PPy nanoarrays on carbon cloth for solid-state asymmetric supercapacitors, *Angew. Chem. Int. Ed.*, 2017, **56**, 1105−1110.

5 X. F. Lu, X. Y. Chen, W. Zhou, Y. X. Tong and G. R. Li, α-Fe_2O_3@PANI core−shell nanowire arrays as negative electrodes for asymmetric supercapacitors, *ACS Appl. Mater. Interfaces*, 2015, **7**, 14843−14850.

6 S. M. Peng, L. Yu, B. Lan, M. Sun, G. Cheng, S. H. Liao, H. Cao and Y. L. Deng, Low-cost superior solid-state symmetric supercapacitors based on hematite nanocrystals, *Nanotechnology*, 2016, **27**, 505404−505416.

7 K. Chi, Z. Y. Zhang, Q. Y. Lv, C. Y. Xie, J. Xiao, F. Xiao and S. Wang, Well-ordered oxygen-deficient $CoMoO_4$ and Fe_2O_3 nanoplate arrays on 3D graphene foam: Toward flexible asymmetric supercapacitors with enhanced capacitive properties, *ACS Appl. Mater. Interfaces*, 2017, **9**, 6044-6053.

8 Y. X. Zeng, Y. Han, Y. T. Zhao, Y. Zeng, M. H. Yu, Y. J. Liu, H. L. Tang, Y. X. Tong and X. H. Lu, Advanced Ti-doped Fe_2O_3@PEDOT core/shell anode for

high-energy asymmetric supercapacitors, *Adv. Energy Mater.*, 2015, **5**, 1402176–1402183.

9 H. W. Wang, Z. J. Xu, H. Yi, H. G. Wei, Z. H. Guo and X. F. Wang, One-step preparation of single-crystalline Fe_2O_3 particles/graphene composite hydrogels as high performance anode materials for supercapacitors, *Nano Energy*, 2014, **7**, 86−96.

10 P. H. Yang, Y. Ding, Z. Y. Lin, Z. W. Chen, Y. Z. Li, P. F. Qiang, M. Ebrahimi, W. J. Mai, C. P. Wong and Z. L. Wang, Low-cost high-performance solid-state asymmetric supercapacitors based on MnO_2 nanowires and Fe_2O_3 nanotubes, *Nano Lett.*, 2014, **14**, 731-736.

11 X. H. Lu, Y. X. Zeng, M. H. Yu, T. Zhai, C. L. Liang, S. L. Xie, M. S. Balogun and Y. X. Tong, Oxygen-deficient hematite nanorods as high-performance and novel negative electrodes for flexible asymmetric supercapacitors, *Adv. Mater.*, 2014, **26**, 3148–3155.

12 Y. Jiao, Y. Liu, B. Yin, S. W. Zhang, F. Y. Qu and X. Wu, Hybrid α-Fe_2O_3@NiO heterostructures for flexible and high performance supercapacitor electrodes and visible light driven photocatalysts, *Nano Energy*, 2014, **10**, 90−98.

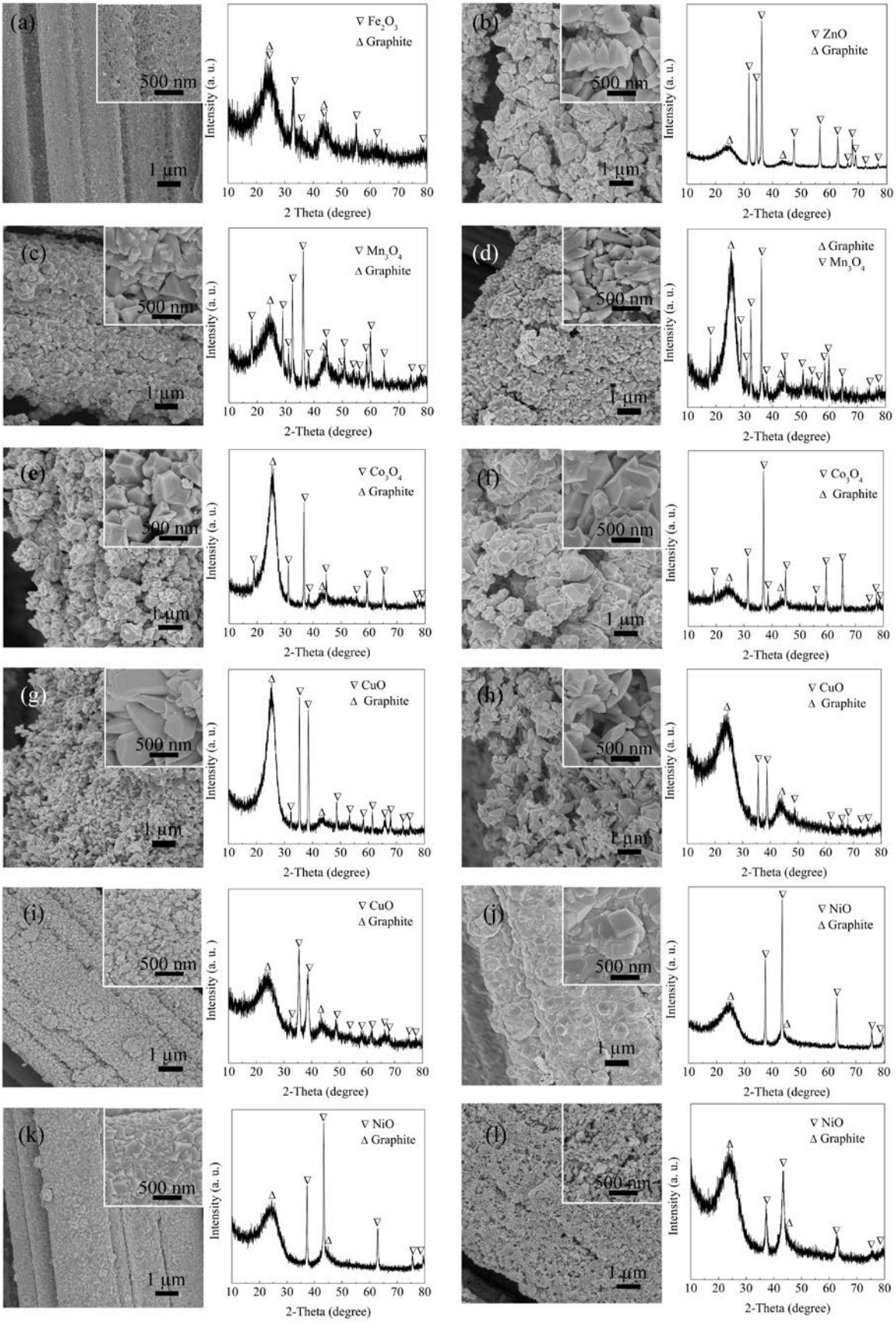
(a)
500 nm
1 μm
∇ Fe_2O_3
Δ Graphite
Intensity (a. u.)
2 Theta (degree)
(b)
500 nm
1 μm
∇ ZnO
Δ Graphite
Intensity (a. u.)
2-Theta (degree)
(c)
500 nm
1 μm
∇ Mn_3O_4
Δ Graphite
Intensity (a. u.)
2-Theta (degree)
(d)
500 nm
1 μm
Δ Graphite
∇ Mn_3O_4
Intensity (a. u.)
2-Theta (degree)
(e)
500 nm
1 μm
∇ Co_3O_4
Δ Graphite
Intensity (a. u.)
2-Theta (degree)
(f)
500 nm
1 μm
∇ Co_3O_4
Δ Graphite
Intensity (a. u.)
2-Theta (degree)
(g)
500 nm
1 μm
∇ CuO
Δ Graphite
Intensity (a. u.)
2-Theta (degree)
(h)
500 nm
1 μm
∇ CuO
Δ Graphite
Intensity (a. u.)
2-Theta (degree)
(i)
500 nm
1 μm
∇ CuO
Δ Graphite
Intensity (a. u.)
2-Theta (degree)
(j)
500 nm
1 μm
∇ NiO
Δ Graphite
Intensity (a. u.)
2-Theta (degree)
(k)
500 nm
1 μm
∇ NiO
Δ Graphite
Intensity (a. u.)
2-Theta (degree)
(l)
500 nm
1 μm
∇ NiO
Δ Graphite
Intensity (a. u.)
2-Theta (degree)

Figure S1. FESEM images (left) and XRD patterns (right) of MOs/CC. (a) Fe_2O_3@CC obtained using $Fe_2(SO_4)_3$; (b) ZnO@CC obtained using $ZnSO_4$; Mn_3O_4@CC obtained using (c) $MnCl_2$ and (d) $MnSO_4$, respectively; Co_3O_4@CC samples obtained using (e) $Co(NO_3)_2$ and (f) $CoCl_2$, respectively; CuO@CC obtained using (g) $Cu(NO_3)_2$, (h) $CuCl_2$ and (i) $CuSO_4$, respectively; NiO@CC obtained using (j) $Ni(NO_3)_2$, (k) $NiCl_2$ and (l) $NiSO_4$, respectively.

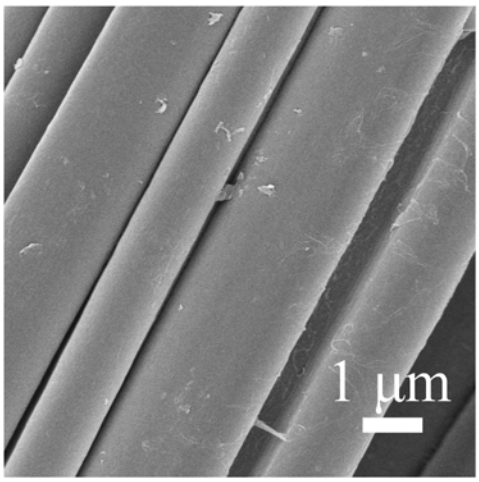

Figure S2. FESEM image of blank carbon cloth substrate.

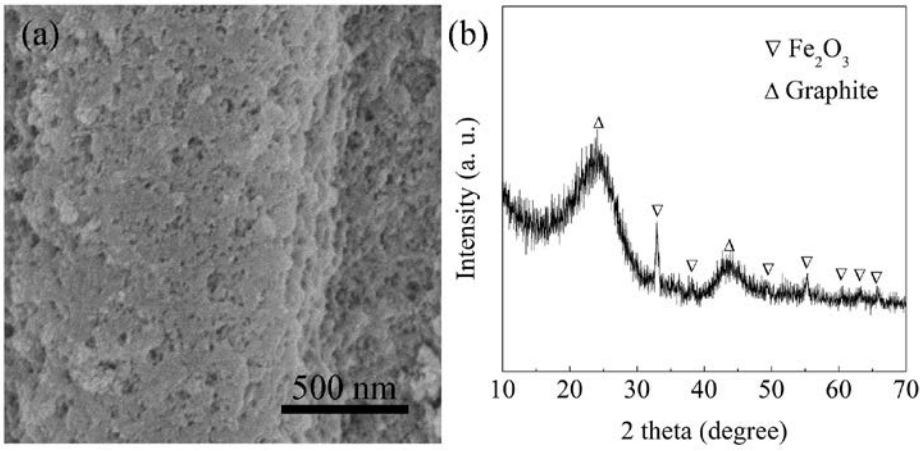

Figure S3. (a) FESEM image and (b) XRD pattern of the Fe_2O_3@CC obtained using 2.5 g $NaNO_3$ and 0.3 mmol $FeCl_3$.

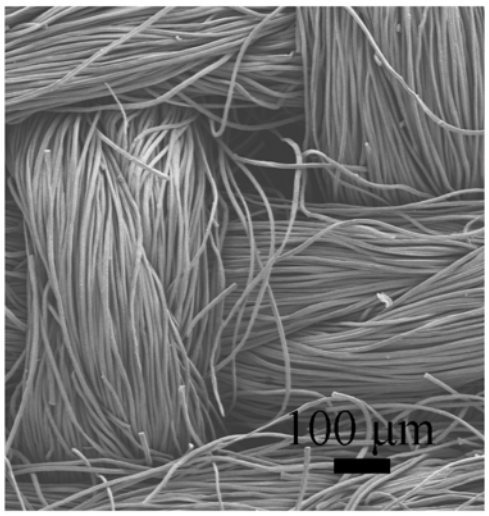

Figure S4. FESEM images of the 0.9-Fe_2O_3@CC electrode.

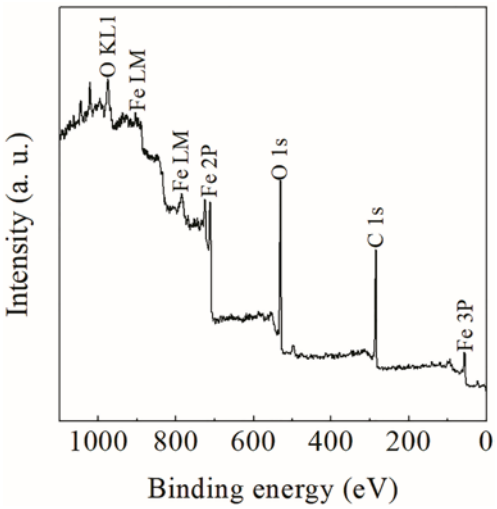

Figure S5. Full scan XPS spectrum of the 0.9-Fe_2O_3@CC electrode.

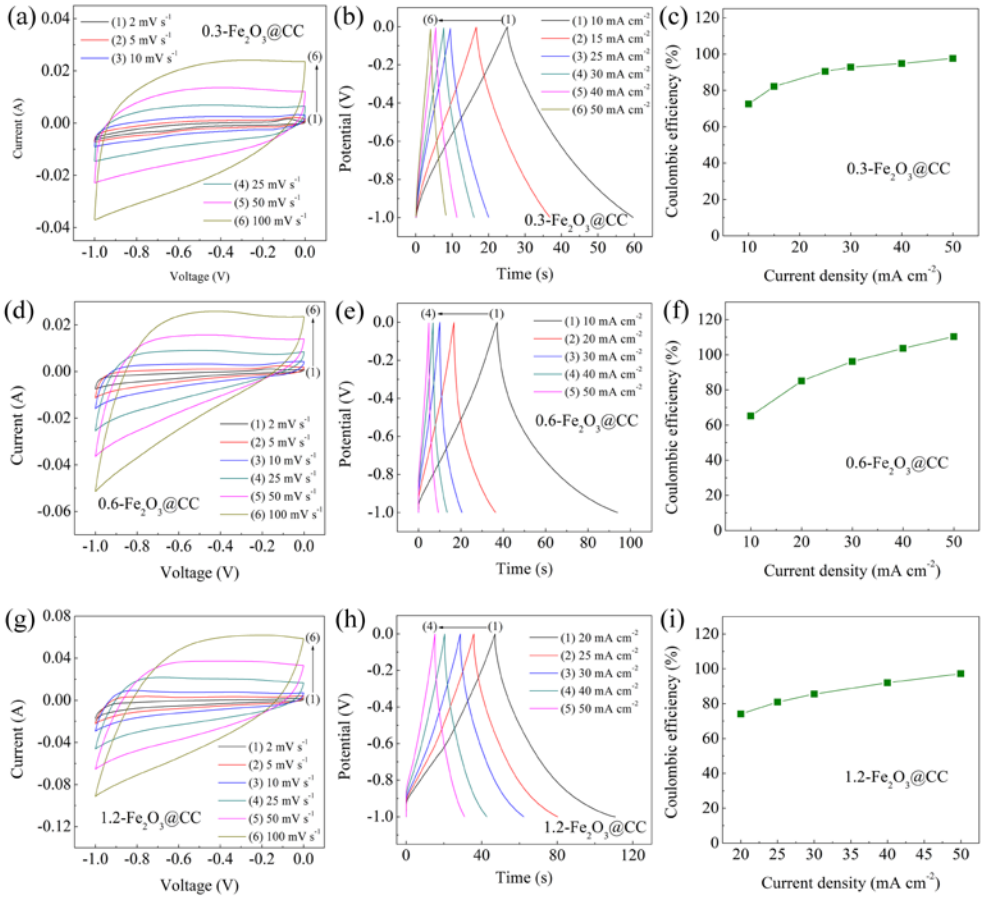

Figure S6. (a, d and g) CV curves at virous scan rates, (b, e and h) GCD curves at different current densities and (c, f and i) coulombic efficiencies of the 0.3-Fe_2O_3@CC, 0.6-Fe_2O_3@CC and 1.2-Fe_2O_3@CC, respectively.

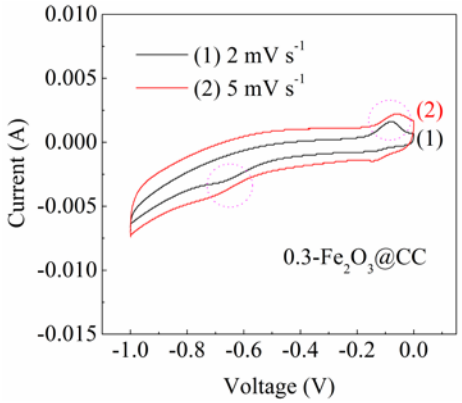

Figure S7. CV curves of the 0.3-Fe_2O_3@CC electrode at scan rates of 2 and 5 mV s^{-1}. The circled region shows the redox peaks.

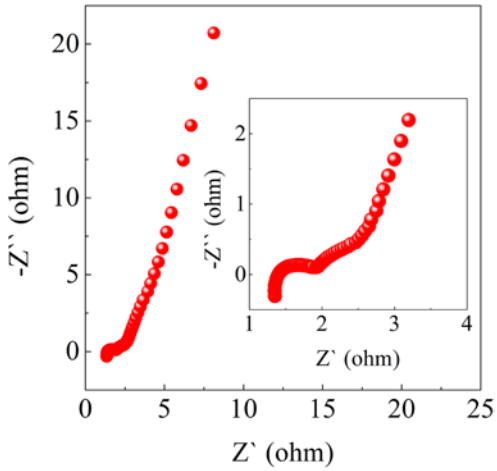

Figure S8. The Nyquist plots of the 0.9-Fe_2O_3@CC electrode. The inset is the enlarged plots at high frequency.

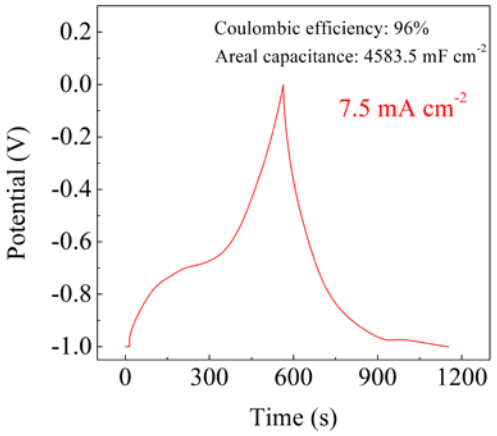

Figure S9. The GCD curve of the 0.9-Fe_2O_3@CC electrode at a current density of 7.5 mA cm^{-2}. The areal capacitance is 4583.5 mF cm^{-2}. The coulombic efficiency is ca. 96%.

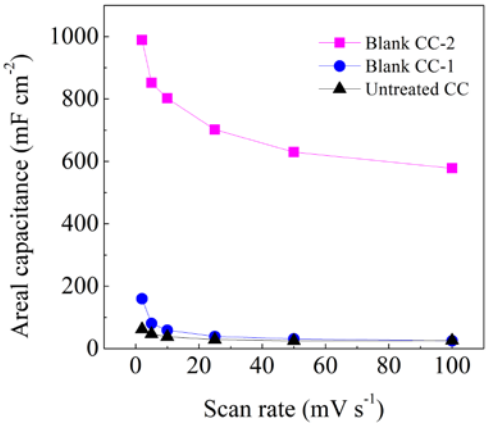

Figure S10. Areal capacitances of the untreated CC, the blank CC-1 and the blank CC-2 electrodes within -1−0 V in 6M KOH electrolyte.

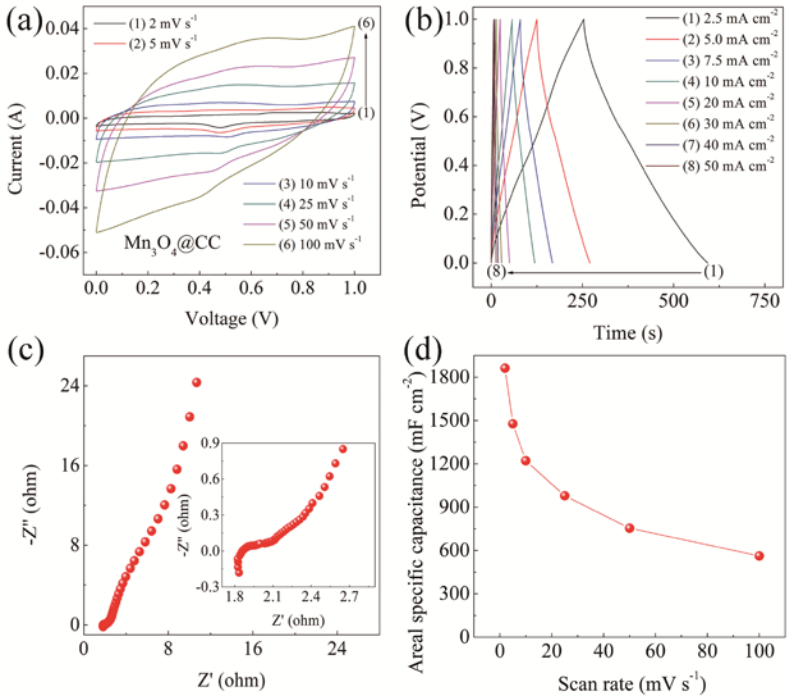

Figure S11. (a) CV and (b) GCD curves of the Mn_3O_4@CC electrode at different scan rates and current densities, respectively. (c) the Nyquist plots; the inset is the enlarged plots at high frequency. (d) Areal specific capacitance at different scan rates.